

# Fenton Degradation of Ofloxacin using a Montmorillonite-Fe<sub>3</sub>O<sub>4</sub> Composite

Alamri Rahmah Dhahawi Ahmad, Saifullahi Shehu Imam, Wen Da Oh and Rohana Adnan\*

School of Chemical Sciences, Universiti Sains Malaysia, 11800 Penang, Malaysia; rahalamri@student.usm.my (A.R.D.A.); ssimam.chm@buk.edu.ng (S.S.I.); ohwenda@usm.my (W.D.O.);

\* Correspondence: r\_adnan@usm.my

† Presented at the 1st International Electronic Conference on Catalysis Sciences, 15–30 November 2020;

Available online: <https://eccs2020.sciforum.net/>

Published: 10 November 2020

**Abstract:** In this work, FeM composites consisting of montmorillonite and variable amounts of Fe<sub>3</sub>O<sub>4</sub> were successfully synthesized via a facile co-precipitation process. They were characterized using X-ray photoelectron spectroscopy (XPS), field emission scanning electron microscope (FESEM), energy dispersive X-ray spectroscopy (EDX), transmission electron microscope (TEM), N<sub>2</sub> adsorption-desorption, and Fourier transform infrared spectroscopy (FT-IR) techniques to explain the effect of Fe<sub>3</sub>O<sub>4</sub> content on the physicochemical properties of the Fe<sub>3</sub>O<sub>4</sub>-montmorillonite (FeM) composites. The FeM composites were subsequently used as heterogeneous Fenton catalysts to activate green oxidant (H<sub>2</sub>O<sub>2</sub>) for the subsequent degradation of ofloxacin (OFL) antibiotic. The efficiency of the FeM composites was studied by varying various parameters of Fe<sub>3</sub>O<sub>4</sub> loading on montmorillonite, catalyst dosage, initial solution pH, initial OFL concentration, different oxidants, H<sub>2</sub>O<sub>2</sub> dosage, reaction temperature, inorganic salts, and solar irradiation. Under the conditions of 0.75 g/L FeM-10, 5 mL/L H<sub>2</sub>O<sub>2</sub>, and natural pH, almost 81 % of 50 mg/L of OFL was removed within 120 min in the dark, while total organic carbon (TOC) reduction was about 56 %. Moreover, the FeM-10 composite maintained high efficiency and was stable even after four continuous cycles, making it a promising candidate in real wastewater remediation.

**Keywords:** Fenton degradation; Ofloxacin; Fe<sub>3</sub>O<sub>4</sub>; Montmorillonite; Heterogeneous

## 1. Introduction

For the past few years, the high consumption of antibiotics has resulted in their continuous detection in surface, ground, drinking, and wastewater around the world [1]. Among the antibiotics, ofloxacin (OFL) is an extensively used 2nd-generation fluoroquinolone due to its good antibacterial activity [2,3]. However, approximately 90% is excreted via urination in its original form 48 h after administration [4]. Unfortunately, OFL is still being detected in wastewater even after conventional treatment [5]. Thus, the development of an effective method for the removal of OFL from wastewater becomes imperative.

The Fenton reaction has gained widespread acceptance due to its efficiency in degrading and even mineralizing persistent organic contaminants with the highly reactive hydroxyl radicals ( $\bullet\text{OH}$ ) [6]. To overcome the shortcomings of the homogeneous Fenton process, heterogeneous Fenton catalysts such as Fe<sub>3</sub>O<sub>4</sub> nanoparticles [7] and Fe-Mn oxide [8] have been proposed. Among the catalysts, Fe<sub>3</sub>O<sub>4</sub> nanoparticles have received significant attention due to their low toxicity and biocompatibility properties [9]. Moreover, another type of potential heterogeneous catalyst that has gained attention involved immobilization of Fe<sub>3</sub>O<sub>4</sub> on solid supports [10]. Although such immobilization prevents agglomeration and enhances the dispersibility of Fe<sub>3</sub>O<sub>4</sub>, the choice of appropriate support is critical [11]. In the present study, a heterogeneous catalyst (Fe<sub>3</sub>O<sub>4</sub>-montmorillonite (FeM)) was synthesized via a facile co-precipitation process and used to activate green oxidant (H<sub>2</sub>O<sub>2</sub>) for the subsequent degradation of ofloxacin (OFL).

## 2. Experimental

### 2.1. Synthesis of Fe<sub>3</sub>O<sub>4</sub>-Montmorillonite (FeM) Composites

Fe<sub>3</sub>O<sub>4</sub>-Montmorillonite (FeM) composites were synthesized via a facile co-precipitation process [12]. Initially, a solution of equimolar amounts of ferric salt and ferrous salt was prepared by dissolving (3, 5, 8, 10, and 15 mmol) of FeCl<sub>3</sub>·6H<sub>2</sub>O and FeSO<sub>4</sub>·7H<sub>2</sub>O in 60 mL of 10 mmol L<sup>-1</sup> aqueous HCl solution, and heated to 80 °C. 0.5 g of montmorillonite was then added and further stirred for 1 h. Then 40 mL of 3.0 mol L<sup>-1</sup> aqueous ammonia (precipitant) was slowly added and stirred for 2 h. After that, the product was collected, washed several times with distilled water and absolute ethanol. Finally, the product was dried in an oven at 60 °C overnight and labelled FeM-3, FeM-5, FeM-8, FeM-10, and FeM-15, based on the equimolar amount of iron salts used in synthesis.

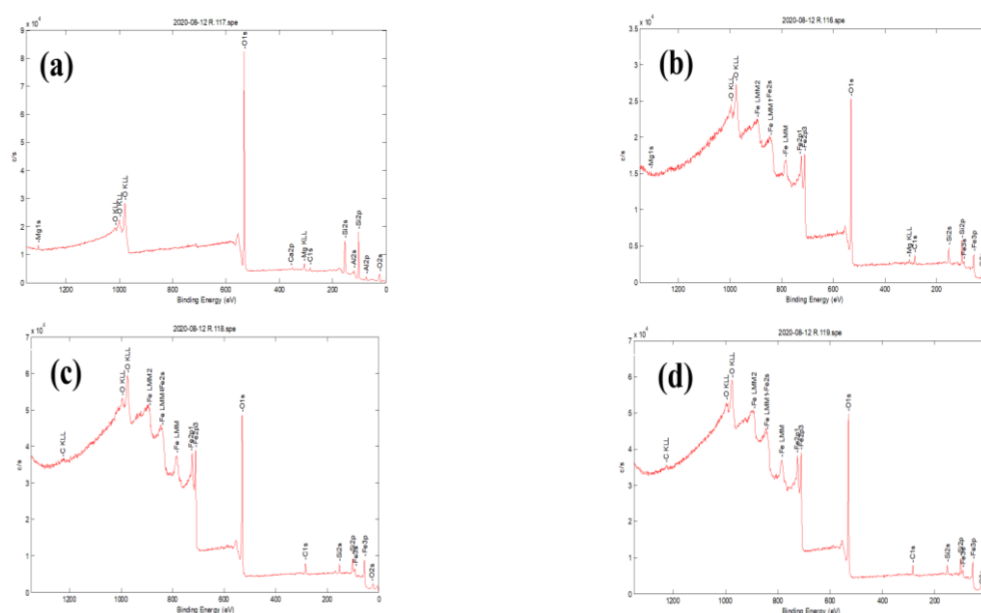
### 2.2. Fenton Reaction

Typically, 0.075 g of the catalyst was placed into 100 mL of 50 mg/L OFL solution, and the suspension was stirred in the dark for 30 min to establish adsorption/desorption equilibrium. Subsequently, 0.5 mL of H<sub>2</sub>O<sub>2</sub> (30% w/w) was added to activate the Fenton reaction. After a certain period, 5 mL of the supernatant was collected for centrifugation, and the concentration of OFL was then analyzed using Shimadzu UV 2600 spectrophotometer (version 1.03 operating using UV probe 2.42) at an absorption wavelength of 286 nm. Total organic carbon (TOC) was determined using Shimadzu TOC-L analyzer.

## 3. Results and Discussion

### 3.1. Characterization of Bare Montmorillonite and Fe<sub>3</sub>O<sub>4</sub>-Montmorillonite Composites

XPS spectra in Figure 1. revealed that Mg, O, C, Ca, Si, and Al existed on the surface of bare montmorillonite. In addition to Mg, O, C, Ca, Si and Al, the spectra of FeM composites confirms the existence of Fe. For instance, Fe 2p<sub>3/2</sub> and Fe 2p<sub>1/2</sub> peaks appeared at binding energies of about 710 and 725 eV [13,14]. Furthermore, the peak at about 94 eV is attributed to the existence of Fe<sub>3</sub>O<sub>4</sub> [12]. This indicates that the iron oxide in the FeM composites is Fe<sub>3</sub>O<sub>4</sub>.



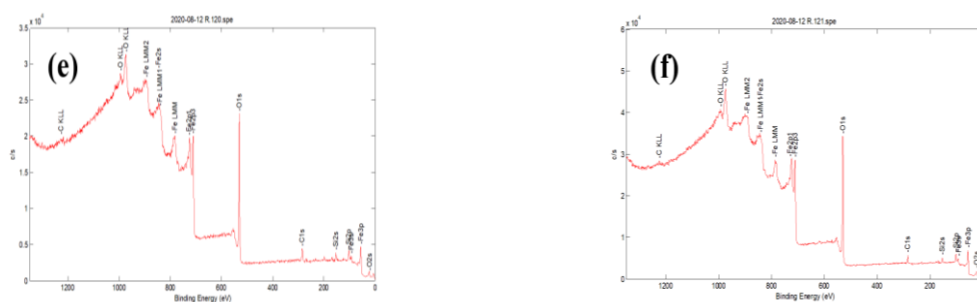


**Figure 1.** XPS spectra of montmorillonite (a), FeM-3 (b), FeM-5 (c), FeM-8 (d), FeM-10 (e) and FeM-15 (f).

FESEM revealed that bare montmorillonite is smooth with irregular flake-like particles. In contrast, the images of FeM composites showed the presence of  $\text{Fe}_3\text{O}_4$ . In the case of FeM-3, FeM-5, and FeM-8 composites, montmorillonite remained visible due to the low amount of  $\text{Fe}_3\text{O}_4$  immobilized. However, the surface of montmorillonite in FeM-10 and FeM-15 composites is wholly covered due to the high amount of  $\text{Fe}_3\text{O}_4$  immobilized in the composites.

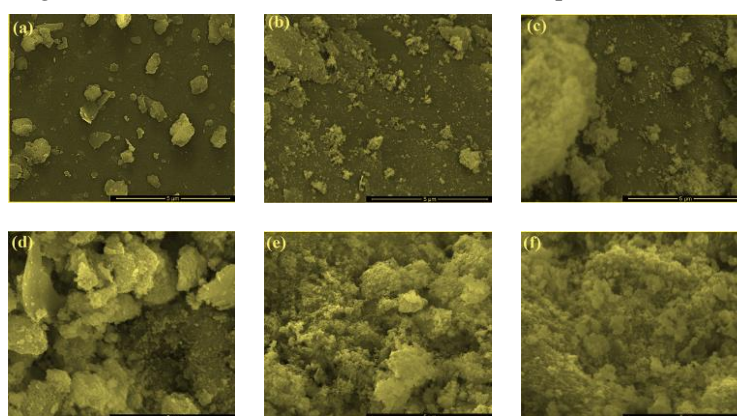


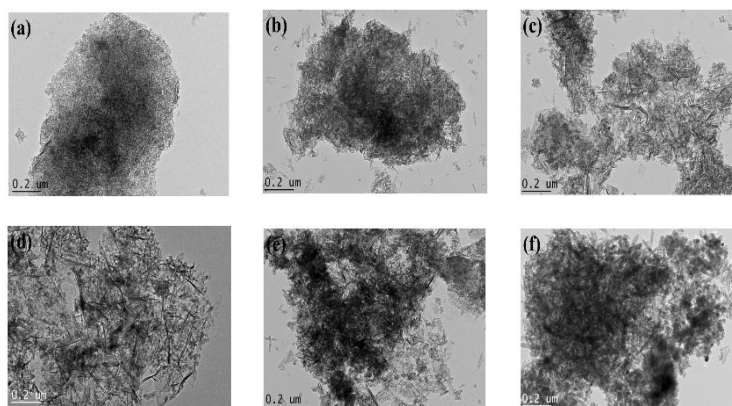
**Figure 2.** FESEM images of montmorillonite (a), FeM-3 (b), FeM-5 (c), FeM-8 (d), FeM-10 (e) and FeM-15 (f).

Furthermore, from the EDX data presented in Table 1, the percentage of iron on the surface of the FeM composites keeps on increasing. The absence of  $\text{K}^+$  and  $\text{Mg}^{2+}$  in the FeM composites is due to the exchange of these ions with  $\text{Fe}^{2+}$  and  $\text{Fe}^{3+}$  ions in the interlayer of montmorillonite [15].

**Table 1.** Composition, surface area and pore volume of montmorillonite and FeM composites.

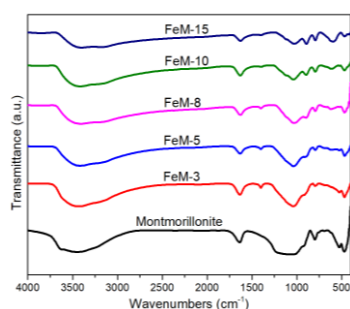
| Sample          | Al % | Si %  | K %  | Mg % | O %   | Fe %  | BET surface area (m <sup>2</sup> /g) | Pore volume (cm <sup>3</sup> /g) |
|-----------------|------|-------|------|------|-------|-------|--------------------------------------|----------------------------------|
| Montmorillonite | 9.21 | 33.06 | 4.10 | 1.11 | 52.52 | -     | 258.108                              | 0.423                            |
| FeM-3           | 1.61 | 17.76 | -    | -    | 37.36 | 43.19 | 247.944                              | 0.634                            |
| FeM-5           | 1.31 | 10.17 | -    | -    | 36.92 | 51.60 | 192.118                              | 0.602                            |
| FeM-8           | 0.83 | 6.58  | -    | -    | 33.93 | 58.66 | 163.552                              | 0.384                            |
| FeM-10          | 0.47 | 5.24  | -    | -    | 33.73 | 60.54 | 161.800                              | 0.363                            |
| FeM-15          | 0.18 | 2.71  | -    | -    | 32.96 | 64.15 | 113.186                              | 0.312                            |

The morphology was further studied using TEM, and the results are shown in Figure 3. Bare montmorillonite in Figure 3(a) has a smooth surface compared to FeM composites in Figures 3(b-f). Such an effect in the case of FeM composites is because  $\text{Fe}_3\text{O}_4$  particles have been deposited and aggregated on the surface of montmorillonite.



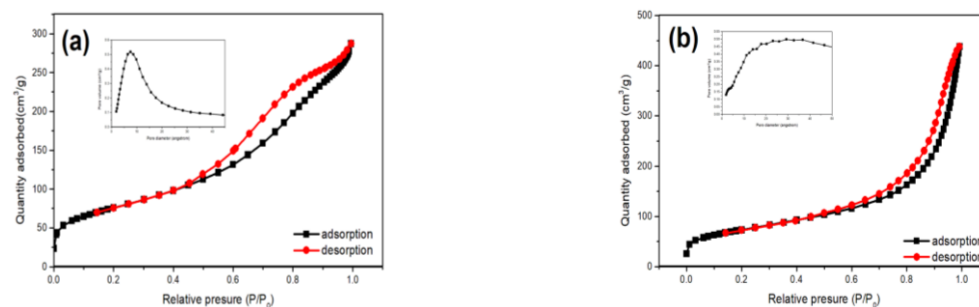
**Figure 3.** TEM images of montmorillonite (a), FeM-3 (b), FeM-5 (c), FeM-8 (d), FeM-10 (e) and FeM-15 (f).

FTIR spectra are presented in Figure 4. Bare montmorillonite has bands at about 450 and 523  $\text{cm}^{-1}$  due to Al–O–Si and Si–O–Si deformations [16]. The band at about 916  $\text{cm}^{-1}$  is due to Al–Al–OH bending vibration, while that at 1050  $\text{cm}^{-1}$  is attributed to the Si–O stretching [17,18]. In the case of the FeM composites, peaks within 1090–400  $\text{cm}^{-1}$  are less intense compared to those of bare montmorillonite. This indicates that Fe could link with Al–O and Si–O in montmorillonite [19].



**Figure 4.** FTIR spectra of bare montmorillonite and FeM composites.

Nitrogen adsorption-desorption isotherms and BJH pore size distributions are shown in Figure 5. The isotherms are identified as type IV with H3 hysteresis loop in the range of 0.5–0.98, a characteristic of mesoporous materials [20]. Furthermore, the BET surface areas and pore volumes of bare montmorillonite and FeM composites are presented in Table 1. FeM composites have a lower BET surface area compared to bare montmorillonite. This could be attributed to the  $\text{Fe}_3\text{O}_4$  in pores or on the surface of montmorillonite.



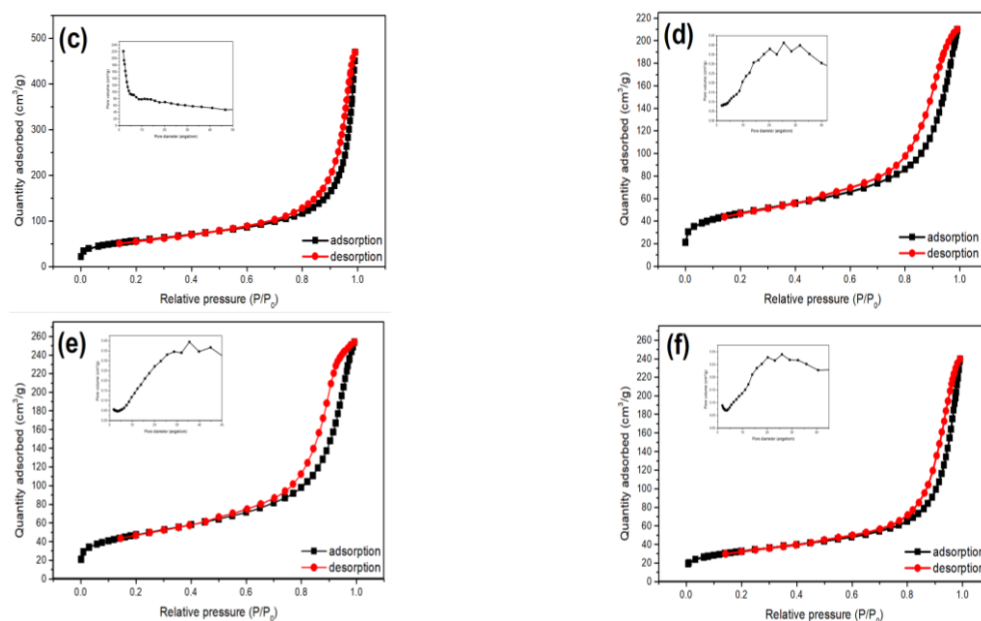


**Figure 5.** N<sub>2</sub> adsorption – desorption isotherms and the corresponding pore size distribution (insets) for montmorillonite (a), FeM-3 (b), FeM-5 (c), FeM-8 (d), FeM-10 (e) and FeM-15 (f) composites.

### 3.2. Fenton Reaction

#### 3.2.1. OFL Removal in Different Processes

Control study was conducted, and the results are shown in Figure 6. Due to the low oxidation potential of H<sub>2</sub>O<sub>2</sub>, the percentage removal in the presence of H<sub>2</sub>O<sub>2</sub> was negligible [10]. Bare montmorillonite could remove more than 50% of OFL [50 mg/L] within 120 min, and the removal was almost maintained even after the introduction of H<sub>2</sub>O<sub>2</sub>. In the case of FeM composite, the percentage removal recorded in the presence of H<sub>2</sub>O<sub>2</sub> was much higher than the removal in the absence of H<sub>2</sub>O<sub>2</sub>, as FeM could activate H<sub>2</sub>O<sub>2</sub>.

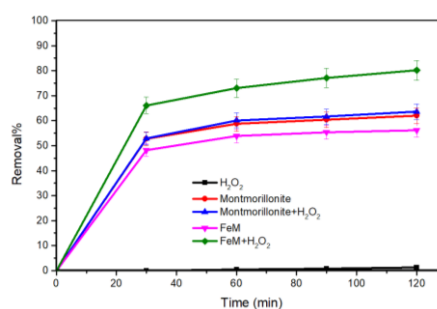


**Figure 6.** OFL removal in different processes.

#### 3.2.2. Influence of Process Variables

Figure 7a shows the effect of Fe<sub>3</sub>O<sub>4</sub> loading on montmorillonite on the degradation of OFL. As the amount of Fe<sub>3</sub>O<sub>4</sub> increases from 3–10 mmol, the percentage removal also increases, due to the increased production of hydroxyl radicals. Beyond 10 mmol, the percentage removal decreases, as high amount of iron ions serve as hydroxyl radicals scavenger [21]. The effect of catalyst dosage shown in Figure 7b revealed that, as the dose of FeM-10 composite increases from 0.025–0.1 g, the percentage removal also increases due to the increase in surface area or active sites for pollutant reactions. However, the percentage removal recorded using 1 g/L of FeM-10 composite is not very much different from the removal using 0.75 g/L, due to the hydroxyl scavenging effect by the high amount of iron ions. Figure 7c shows the effect of initial solution pH on the Fenton reaction. The

performance was favourable at low pH, and keeps on retarding with increase in pH. This is because hydroxyl radicals have lower redox potential in basic medium and  $\text{H}_2\text{O}_2$  may be consumed without the production of hydroxyl radicals [22]. The results for the effect of initial OFL concentration on the efficiency of FeM-10 composite are presented in Figure 7d. The percentage removal keeps on decreasing with increase in initial concentration due to the unavailability of the active sites of FeM-10 composite. Figure 7e presents the effect of different oxidants on the Fenton reaction. The percentage removal in the presence of PDS and  $\text{H}_2\text{O}_2$ , was higher than the removal in the presence of PMS. This could be attributed to the inherent pH of aqueous OFL solution ( $\text{pH} = 9$ ), as self-dissociation of PMS occur at elevated pH through non-radical pathways [23]. The effect of  $\text{H}_2\text{O}_2$  dosage on the Fenton reaction was also studied, and the results are presented in Figure 7f. The percentage removal increases with an increase in dosage from 1–5ml/L, but decreases beyond 5ml/L, as surplus amount of  $\text{H}_2\text{O}_2$  might consume hydroxyl radicals. [22] Figure 7g shows the effect of temperature on the Fenton reaction. While the temperature was varied from 25–60 °C, the percentage removal remained virtually unchanged. As such, higher reaction temperatures were not useful for increasing the degradation of OFL by FeM-10 composite. The results for the effect of inorganic salts on the Fenton reaction are shown in Figure 7 h. There was a minor decrease in the percentage of OFL removed in the presence of the inorganic salts used. Such a decrease could be because  $\text{Cl}^-$  serves as hydroxyl radical scavenger [24].

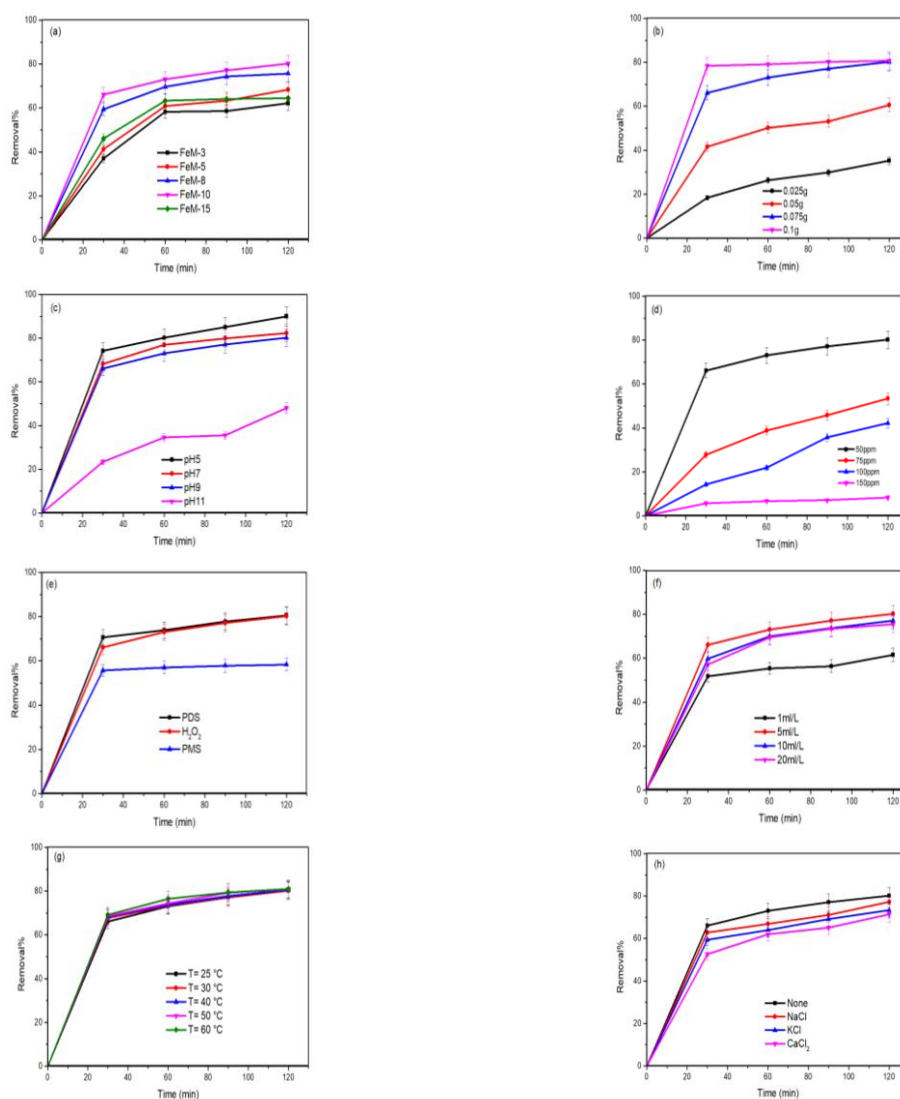


**Figure 7.** Effects of (a) Fe<sub>3</sub>O<sub>4</sub> loading on montmorillonite, (b) catalyst dosage, (c) initial solution pH, (d) initial OFL concentration, (e) different oxidants, (f) H<sub>2</sub>O<sub>2</sub> dosage, (g) reaction temperature, and (h) inorganic salts.

### 3.2.3. Photo-Fenton Catalytic Activity

The photo-Fenton activity of FeM-10 composite towards the degradation of OFL antibiotic was studied using optimized conditions, under solar irradiation, and the results are shown in Figure 8. The amount of OFL oxidized under solar irradiation after 120 min was minimal. However, the percentage increased upon the introduction of H<sub>2</sub>O<sub>2</sub>. This is due to the formation of hydroxyl radicals through the direct photolysis of H<sub>2</sub>O<sub>2</sub> [25]. Furthermore, the percentage of OFL removed via adsorption by the FeM-10 composite was about 56%. However, the percentage increased to 76% under solar irradiation, due to the photocatalytic effect of the FeM-10 composite. Finally, compared to the percentage removal recorded via Fenton process (about 81%), the performance via photo-Fenton degradation was higher (about 92%). This indicates that FeM-10 composite is an efficient heterogeneous photo-Fenton catalyst under solar irradiation.

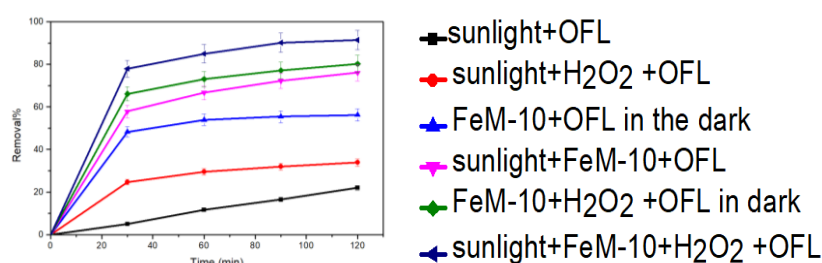


**Figure 8.** Degradation of OFL under different conditions.

### 3.2.4. Reusability and Stability Studies

The recyclability of FeM-10 composite was also studied, and the results are shown in Figure 9a. It can be seen that the catalyst still maintains high efficiency after every cycle. The slight decrease might be attributed to the adsorption of OFL byproducts on the surface of FeM-composite. Meanwhile, the FTIR spectrum of the FeM-10 composite (Figure 9b) after the five cycles is in good agreement with that of fresh FeM-10 composite, as no impurity peaks were detected.

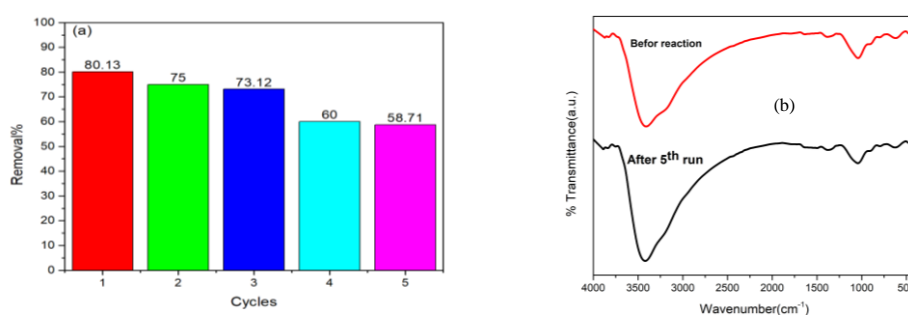


**Figure 9.** Recycling performance of FeM-10 composite in the degradation of OFL (a) FTIR spectra of FeM-10 composite before and after five cycles (b).

## 4. Conclusion

Fe<sub>3</sub>O<sub>4</sub>-montmorillonite composites have been synthesized via facile co-precipitation process. The effect of Fe<sub>3</sub>O<sub>4</sub> loading on montmorillonite was characterized using various techniques. The FeM composites were subsequently used as heterogeneous Fenton catalysts to activate green oxidant (H<sub>2</sub>O<sub>2</sub>) for the subsequent degradation of ofloxacin (OFL) antibiotic. Under the conditions of 0.75 g/L FeM-10, 5 mL/L H<sub>2</sub>O<sub>2</sub>, and natural pH, almost 81% of 50 mg/L of OFL was degraded within 120 min in the dark. However, the removal increased to about 92% during photo-Fenton process. In addition,

the FeM-10 composite maintained reasonable efficiency even after five cycles, therefore could be a promising heterogeneous catalyst for the activation of H<sub>2</sub>O<sub>2</sub> to degrade pollutants, including OFL antibiotic.

**Author Contributions:** Conceptualization, methodology, resources, and writing—review and editing, R.A.; writing—review and editing, W.D.O. and S.S.I.; investigation and writing—original draft preparation, A.R.D.A. . All authors have read and agreed to the published version of the manuscript.

**Funding:** The authors gratefully acknowledged the financial support from Universiti Sains Malaysia under RUI Grant No. 1001/PKIMIA/8011117.

**Acknowledgment:** The authors gratefully thank Universiti Sains Malaysia for the financial support provided under RUI Grant No. 1001/PKIMIA/8011117.

**Conflicts of Interest:** The authors declare no conflict of interest. The funders had no role in the design of the study; in the collection, analyses, or interpretation of data; in the writing of the manuscript, or in the decision to publish the results.

## References

1. Chen, P.; Blaney, L.; Cagnetta, G.; Huang, J.; Wang, B.; Wang, Y.; Deng, S.; Yu, G. Degradation of ofloxacin by perylene diimide supramolecular nanofiber sunlight-driven photocatalysis. *Environmental science & technology* **2019**, *53*, 1564–1575.
2. Liu, J.; Wu, X.; Liu, J.; Zhang, C.; Hu, Q.; Hou, X. Ofloxacin degradation by Fe<sub>3</sub>O<sub>4</sub>-CeO<sub>2</sub>/AC Fenton-like system: Optimization, kinetics, and degradation pathways. *Molecular Catalysis* **2019**, *465*, 61–67.
3. Zhao, G.; Ding, J.; Zhou, F.; Chen, X.; Wei, L.; Gao, Q.; Wang, K.; Zhao, Q. Construction of a visible-light-driven magnetic dual Z-scheme BiVO<sub>4</sub>/g-C<sub>3</sub>N<sub>4</sub>/NiFe<sub>2</sub>O<sub>4</sub> photocatalyst for effective removal of ofloxacin: mechanisms and degradation pathway. *Chemical Engineering Journal* **2020**, 126704.
4. Kaur, R.; Kushwaha, J.P.; Singh, N. Electro-catalytic oxidation of ofloxacin antibiotic in continuous reactor: evaluation, transformation products and pathway. *Journal of The Electrochemical Society* **2019**, *166*, H250.
5. Changotra, R.; Guin, J.P.; Khader, S.A.; Varshney, L.; Dhir, A. Electron beam induced degradation of ofloxacin in aqueous solution: kinetics, removal mechanism and cytotoxicity assessment. *Chemical Engineering Journal* **2019**, *356*, 973–984.
6. Tian, Y.; He, X.; Zhou, H.; Tian, X.; Nie, Y.; Zhou, Z.; Yang, C.; Li, Y. Efficient fenton-like degradation of ofloxacin over bimetallic Fe–Cu@ Sepiolite composite. *Chemosphere* **2020**, 127209.
7. Xu, L.; Wang, J. Fenton-like degradation of 2, 4-dichlorophenol using Fe<sub>3</sub>O<sub>4</sub> magnetic nanoparticles. *Applied Catalysis B: Environmental* **2012**, *123*, 117–126.
8. Li, L.; Lai, C.; Huang, F.; Cheng, M.; Zeng, G.; Huang, D.; Li, B.; Liu, S.; Zhang, M.; Qin, L. Degradation of naphthalene with magnetic bio-char activate hydrogen peroxide: synergism of bio-char and Fe–Mn binary oxides. *Water research* **2019**, *160*, 238–248.
9. He, H.; Gao, C. Supraparamagnetic, conductive, and processable multifunctional graphene nanosheets coated with high-density Fe<sub>3</sub>O<sub>4</sub> nanoparticles. *ACS applied materials & interfaces* **2010**, *2*, 3201–3210.
10. Hu, X.; Liu, B.; Deng, Y.; Chen, H.; Luo, S.; Sun, C.; Yang, P.; Yang, S. Adsorption and heterogeneous Fenton degradation of 17 $\alpha$ -methyltestosterone on nano Fe<sub>3</sub>O<sub>4</sub>/MWCNTs in aqueous solution. *Applied Catalysis B: Environmental* **2011**, *107*, 274–283.
11. Zhang, Y.; Chen, Z.; Zhou, L.; Wu, P.; Zhao, Y.; Lai, Y.; Wang, F. Heterogeneous Fenton degradation of bisphenol A using Fe<sub>3</sub>O<sub>4</sub>@  $\beta$ -CD/rGO composite: synergistic effect, principle and way of degradation. *Environmental Pollution* **2019**, *244*, 93–101.

12. Huang, R.; Fang, Z.; Yan, X.; Cheng, W. Heterogeneous sono-Fenton catalytic degradation of bisphenol A by Fe<sub>3</sub>O<sub>4</sub> magnetic nanoparticles under neutral condition. *Chemical Engineering Journal* **2012**, *197*, 242–249.
13. Wilson, D.; Langell, M. XPS analysis of oleylamine/oleic acid capped Fe<sub>3</sub>O<sub>4</sub> nanoparticles as a function of temperature. *Applied Surface Science* **2014**, *303*, 6–13.
14. Zhu, Y.; Tian, L.; Jiang, Z.; Pei, Y.; Xie, S.; Qiao, M.; Fan, K. Heteroepitaxial growth of gold on flowerlike magnetite: An efficacious and magnetically recyclable catalyst for chemoselective hydrogenation of crotonaldehyde to crotyl alcohol. *Journal of catalysis* **2011**, *281*, 106–118.
15. Caglar, B.; Guner, E.K.; Keles, K.; Özdokur, K.V.; Cubuk, O.; Coldur, F.; Caglar, S.; Topcu, C.; Tabak, A. Fe<sub>3</sub>O<sub>4</sub> nanoparticles decorated smectite nanocomposite: Characterization, photocatalytic and electrocatalytic activities. *Solid State Sciences* **2018**, *83*, 122–136.
16. Sharma, P.; Borah, D.J.; Das, P.; Das, M.R. Cationic and anionic dye removal from aqueous solution using montmorillonite clay: evaluation of adsorption parameters and mechanism. *Desalination and Water Treatment* **2016**, *57*, 8372–8388.
17. Ashiq, A.; Sarkar, B.; Adassooriya, N.; Walpita, J.; Rajapaksha, A.U.; Ok, Y.S.; Vithanage, M. Sorption process of municipal solid waste biochar-montmorillonite composite for ciprofloxacin removal in aqueous media. *Chemosphere* **2019**, *236*, 124384.
18. Barreca, S.; Colmenares, J.J.V.; Pace, A.; Orecchio, S.; Pulgarin, C. Neutral solar photo-Fenton degradation of 4-nitrophenol on iron-enriched hybrid montmorillonite-alginate beads (Fe-MABs). *Journal of Photochemistry and Photobiology A: Chemistry* **2014**, *282*, 33–40.
19. Azmi, N.; Ayodele, O.; Vadivelu, V.; Asif, M.; Hameed, B. Fe-modified local clay as effective and reusable heterogeneous photo-Fenton catalyst for the decolorization of Acid Green 25. *Journal of the Taiwan Institute of Chemical Engineers* **2014**, *45*, 1459–1467.
20. Wan, D.; Wang, G.; Li, W.; Wei, X. Investigation into the morphology and structure of magnetic bentonite nanocomposites with their catalytic activity. *Applied Surface Science* **2017**, *413*, 398–407.
21. Hassan, H.; Hameed, B. Fe–clay as effective heterogeneous Fenton catalyst for the decolorization of Reactive Blue 4. *Chemical Engineering Journal* **2011**, *171*, 912–918.
22. Khodadadi, M.; Panahi, A.H.; Al-Musawi, T.J.; Ehrampoush, M.; Mahvi, A. The catalytic activity of FeNi<sub>3</sub>@ SiO<sub>2</sub> magnetic nanoparticles for the degradation of tetracycline in the heterogeneous Fenton-like treatment method. *Journal of Water Process Engineering* **2019**, *32*, 100943.
23. Ji, Y.; Wang, L.; Jiang, M.; Yang, Y.; Yang, P.; Lu, J.; Ferronato, C.; Chovelon, J.-M. Ferrous-activated peroxymonosulfate oxidation of antimicrobial agent sulfaquinoxaline and structurally related compounds in aqueous solution: kinetics, products, and transformation pathways. *Environmental Science and Pollution Research* **2017**, *24*, 19535–19545.
24. Tsuneda, S.; Ishihara, Y.; Hamachi, M.; Hirata, A. Inhibition effect of chlorine ion on hydroxyl radical generation in UV-H<sub>2</sub>O<sub>2</sub> process. *Water science and technology* **2002**, *46*, 33–38.
25. Warang, T.; Patel, N.; Santini, A.; Bazzanella, N.; Kale, A.; Miotello, A. Pulsed laser deposition of Co<sub>3</sub>O<sub>4</sub> nanoparticles assembled coating: Role of substrate temperature to tailor disordered to crystalline phase and related photocatalytic activity in degradation of methylene blue. *Applied Catalysis A: General* **2012**, *423*, 21–27.



